Integration and modeling of IPMC and PVDF for simultaneous actuation and sensing

Zheng Chen[a], Yantao Shen[b], Ning Xi[b] and Xiaobo Tan[a*]

[a]The Smart Microsystems Laboratory
[b]The Robotics and Automation Laboratory
Department of Electrical & Computer Engineering
Michigan State University, East Lansing, MI 48824, USA

E-mail: chenzhe1@egr.msu.edu (Z. Chen), xbtan@msu.edu (X. Tan)

Abstract. Compact sensing methods are desirable for ionic polymer-metal composite (IPMC) actuators in microrobotic and biomedical applications. In this paper a novel sensing scheme for IPMC actuators is proposed by bonding an IPMC and a PVDF (polyvinylidene fluoride) thin film with an insulating layer in-between. The insulating layer thickness is properly designed to minimize the stiffness of the composite IPMC/PVDF structure while reducing the electrical feedthrough coupling between IPMC and PVDF. A distributed circuit model is developed to effectively represent the electrical coupling dynamics, which is then used in real-time compensation for extraction of the true sensing signal. Experimental results show that the developed IPMC/PVDF structure, together with the compensation algorithm, can perform effective, simultaneous actuation and sensing. As the first application, this sensori-actuator has been successfully used for performing and monitoring open-loop micro-injection of living Drosophila embryos.

Submitted to: *Smart Mater. Struct.*

*Corresponding author.

1. Introduction

Ionic polymer-metal composites (IPMCs) form an important category of electroactive polymers which has both built-in actuation and sensing capabilities [1, 2]. Due to their large bending displacement, low driving voltage, resilience, and biocompatibility, IPMCs have been explored for potential applications in biomimetic robotics [3, 4], medical devices [5], and micromanipulators [6, 7, 8]. In most of these applications, *compact* sensing schemes are desired for feedback control of IPMC actuators to ensure precise and safe operation without using bulky, separate sensors. It is intriguing to utilize the inherent sensory property of an IPMC to achieve simultaneous actuation and sensing, like the self-sensing scheme for piezoelectric materials [9]. However, this approach is difficult to implement due to the very small magnitude of the sensing signal compared to the actuation signal (millivolts versus volts) [2] and the nonlinear [10], dynamic [11] sensing responses. Newbury [12] explored the idea of using two IPMCs, mechanically coupled in a side-by-side or bilayer configuration, to perform actuation and sensing. The attempt was reported to be unsuccessful since the sensing signal was buried in the feedthrough signal from actuation [12].

In this paper, to our best knowledge, we are the first one to report the integration of highly actuating IPMC and highly sensitive PVDF for simultaneous actuation and sensing. PVDF is a flexible piezoeletric polymer widely used as sensors and actuators [13]. Although a sensori-actuator made of PVDF alone has been developed in [14, 15], its application to microsystems and biomedical systems is limited due to the high actuation voltage (over 40 V), as opposed to the low actuation voltage (under several volts) needed for IPMC. The thin, soft PVDF layer provides a strong sensing signal while having a minimal impact on the IPMC bending performance. However, the electrical feedthrough from the IPMC actuation signal to the PVDF sensing signal, arising from the proximity of IPMC and PVDF, presents a significant challenge in real-time extraction of the sensing signal. A thicker insulating layer would lead to weaker feedthrough coupling, but at the cost of reduced actuation displacement due to the increased structural stiffness. The stiffening effect caused by the PVDF and insulating layers is investigated through analytic modeling, finite-element computation, and experimental measurement. Good agreement is achieved between analysis, computation, and experiments on the impact of the insulating layer thickness on the IPMC/(insulator)/PVDF structural stiffness. Based on these results, the insulating layer thickness is properly chosen for sound trade-off between minimization of structural stiffness and that of electrical feedthrough.

The electrical feedthrough is still not negligible for the chosen insulator thickness. To fully account for the effect of the feedthrough coupling, we develop a distributed circuit model for the IPMC/(insulator)/PVDF structure. Circuit parameters are determined based on impedance measurement through a nonlinear fitting process. Comparison between Pspice simulation and experimental measurement shows that the model represents well the feedthrough coupling dynamics. A real-time compensation scheme is then implemented using a reduced feedthrough model to extract the correct

sensing signal.

As a biological application, the IPMC/PVDF structure is being investigated for automating the process of Drosophila embryo injection. Genetic modification of Drosophila embryos not only provides scientifically interesting insights, but also offers understanding of biological mechanisms to cure diseases [16]. One of the most important tasks in genetic modification is the injection of substances that affect the makeup of a cell or an organism. Most embryo injections are currently conducted manually and the success rate is quite low (about 2-4 %). As a first step toward the goal of fully automated injection, the proposed IPMC/PVDF structure is used to deliver and monitor the penetration of the Drosophila embryo in an open-loop manner.

The remainder of the paper is organized as follows. The design of the IPMC/PVDF structure and the sensing circuit is described in Section 2. The impact of the stiffening effect due to the PVDF and insulator layers is studied in Section 3. The modeling and compensation methods for the feedthrough coupling phenomenon are presented in Section 4. The experimental setup and results for the micro-injection of living Drosophila embryos are shown in Section 5. Finally, the work is concluded in Section 6.

2. Design of IPMC/PVDF structure and sensing circuit

2.1. IPMC/PVDF structure and sensing circuit

To construct the IPMC/PVDF sensori-actuator, a PVDF film (30 μm thick, Measurement Specialties Inc.) is bonded to an IPMC (340 μm thick, Environmental Robotics Inc.) with an insulating layer (Polyvinyl chloride PVC film, 30 μm thick) in between. The Fast-Cure Elastic Epoxy (Polysciences Inc., Warrington, PA) is used in bonding. The design of the IPMC/PVDF structure is illustrated in Fig. 1, where a picture of the IPMC/PVDF prototype is shown at the bottom.

An IPMC using water as solvent needs to be hydrated to work in air. For the IPMC/PVDF structure, it is not recommended to immerse the sample in water due to the presence of the PVDF. Instead, one can place a damp paper towel on top of the IPMC side of the structure and at the same time apply a uniform compressive stress. This will facilitate uniform hydration of the IPMC while preventing the delamination of the layers. The selected PVDF film has high stability and strong capabilities to resist moisture ($< 0.02\%$ moisture absorption) and most chemicals [17]. All the electrodes of IPMC and PVDF are well insulated and aligned without short circuit during the hydration. Following these properties and facts, the effect of the humidity level on PVDF sensing is not observed to be appreciable. The hydrating procedure is not required if one adopts IPMC samples that use ionic fluids [18] or other non-water-based solvents.

When the IPMC/PVDF structure is bent due to IPMC actuation or external forces, charges are generated on the PVDF, which can be measured by a charge amplifier. Fig. 2 shows a differential charge amplifier which can minimize the common-mode noise. The

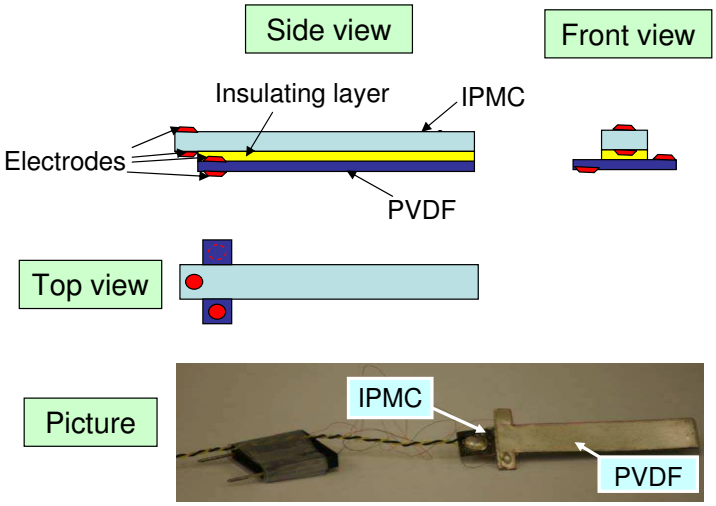

Figure 1. Design of the IPMC/PVDF composite structure.

transfer function of the charge amplifier is described by:

$$\frac{V_o(s)}{Q(s)} = \frac{2R_1 s}{1 + R_1 C_1 s} \frac{R_3}{R_2}, \tag{1}$$

which is a high-pass filter. As $R_1 \to \infty$, the transfer function $\frac{V_o(s)}{Q(s)} \to \frac{2R_3}{C_1 R_2}$. However, in the circuit implementation, R_1 cannot be infinitely large because the bias current of the operational amplifier will saturate the signal output. To accommodate the actuation bandwidth of IPMC (typically below 10 Hz), the R_1 and C_1 values in the circuit are properly chosen so that the cutoff frequency of the charge amplifier is sufficiently low. By picking $R_1 = 5000$ MΩ and $C_1 = 1350$ pF, a cutoff frequency of 0.023 Hz is achieved.

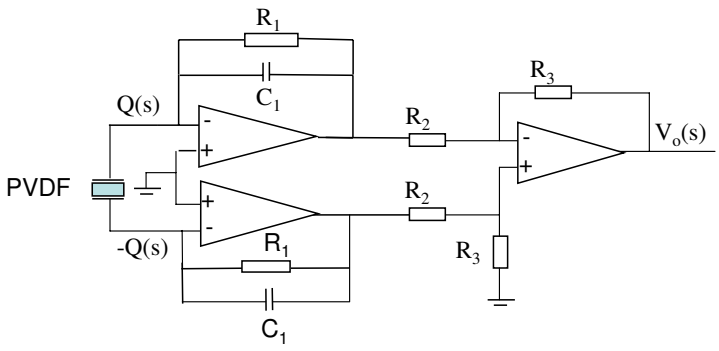

Figure 2. Design of the charge amplifier.

Basically, the charge $Q(s)$ generated by the PVDF is proportional to the bending displacement $Z(s)$ of the beam [19]:

$$Q(s) = GZ(s), \tag{2}$$

where the constant G depends on the transverse piezoelectric coefficient d_{31}, the geometry of the composite beam, and the Young's moduli of individual layers. By

combining (1) and (2), one can obtain the transfer function from $Z(s)$ to $V_o(s)$. A laser displacement sensor (OADM 20I6441/S14F, Baumer Electric) is used for both calibration of the PVDF sensor and validation of the sensing approach. In order to test the charge amplifier circuit, the IPMC/PVDF beam with one end fixed is tapped and then the laser sensor is used to detect the damped vibration of the beam. The measured vibration frequency is 42 Hz, which is much higher than the cutoff frequency of the charge amplifier. Fig. 3(a) shows the charge output of PVDF corresponding to the damped vibration, and Fig. 3(b) demonstrates that the charge signal is almost linear with respect to the bending displacement. These experimental results have validated the performance of the charge amplifier circuit.

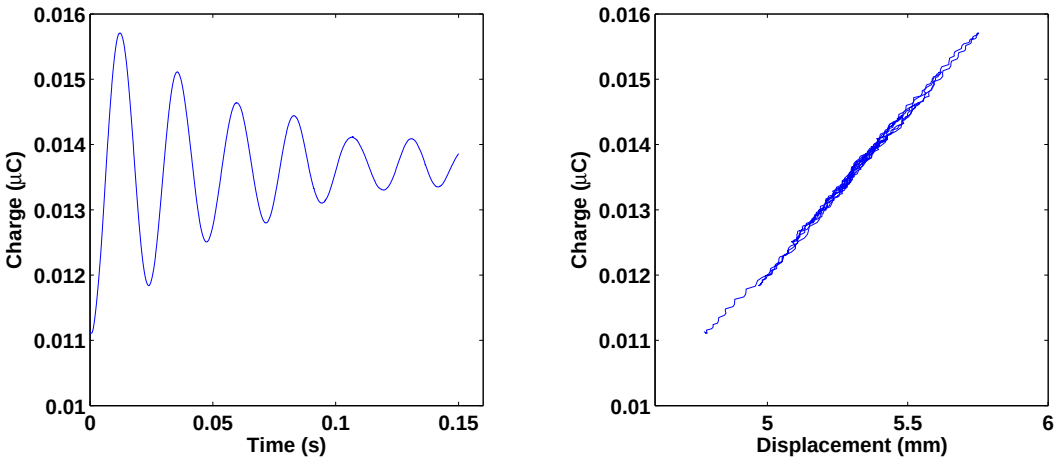

(a) (b)

Figure 3. (a): Charge output of the PVDF corresponding to the damped vibration; (b): Charge output versus the bending displacement.

3. Impact of the stiffening effect and design of the insulator thickness

The additional PVDF and insulating layers make the composite beam stiffer than the IPMC layer itself. It is of interest to understand the impact of this stiffening effect on the bending performance since this will be useful for the optimal IPMC/PVDF structure design. The investigation is conducted by combining analytical modeling, finite element computation, and experiments. Design optimization here is concentrated on the thickness of the insulating layer, but the approach can be used for the design of other parameters, such as the type of material for the insulating layer and the dimensions for IPMC and PVDF.

Fig. 4 illustrates the schematic of the IPMC/PVDF structure and the used notation in the following discussion. The beam stiffness can be characterized by its spring

constant

$$K = \frac{F}{z_{max}}, \tag{3}$$

where F is a quasi-static transverse force applied at the free end of the cantilever beam and z_{max} is the corresponding displacement at the acting point. The spring constant can be calculated analytically using composite beam theory [20]. In Fig. 4, the position of the mechanical neutral axis of the composite beam is given by:

$$h_0 = \frac{\sum_{i=1}^{3} E_i H_i C_i}{\sum_{i=1}^{3} E_i H_i}. \tag{4}$$

Here E_1, E_2 and E_3 are the Young's moduli of IPMC, insulating layer, and PVDF, respectively. H_1, H_2 and H_3 are the thicknesses of those layers. C_1, C_2 and C_3 are the positions of the central axes of the layers, which can be calculated as:

$$C_1 = H_1/2, \qquad C_2 = H_1 + H_2/2, \qquad C_3 = H_1 + H_2 + H_3/2. \tag{5}$$

The distance between the central axis and the neutral axis can be written as:

$$d_i = |C_i - h_0|, \quad \text{for} \quad i = 1, 2, 3. \tag{6}$$

The moment of inertia of each layer is:

$$I_i = \frac{1}{12} W H_i^3 + W H_i d_i^2, \quad \text{for} \quad i = 1, 2, 3. \tag{7}$$

From the moment balance equation [20],

$$M = \frac{\sum_{i=1}^{3} E_i I_i}{\rho(x)} = F(L - x), \tag{8}$$

where $\rho(x)$ is the radius of curvature. For small bending, the radius of curvature can be given by:

$$\frac{1}{\rho(x)} = \frac{d^2 z}{dx^2}, \tag{9}$$

where $z(x)$ denotes the deflection of the beam along the length x. With the boundary condition $z(0) = 0$ and $\dot{z}(0) = 0$, one gets

$$z(x) = \frac{F}{\sum_{i=1}^{3} E_i I_i} (\frac{L x^2}{2} - \frac{x^3}{6}). \tag{10}$$

Evaluating z at $x = L$ yields the expression of spring constant

$$K = \frac{F}{z_{max}} = (\frac{3 \sum_{i=1}^{3} E_i I_i}{L^3}). \tag{11}$$

Experiments are conducted to measure and compare the spring constants of the IPMC and IPMC/PVDF beams. The IPMC or IPMC/PVDF beam is clamped at one end and is pushed by the tip of a calibrated micro-force sensor which is mounted on a linear actuator. The sensitivity of the micro-force sensor is 9.09 mV/μN $\pm$ 6.5% and its spring constant is 0.264 N/m. A laser displacement sensor measures the bending displacement of the beam z_{max} under the pushing force F. A 20X microscope (FS60,

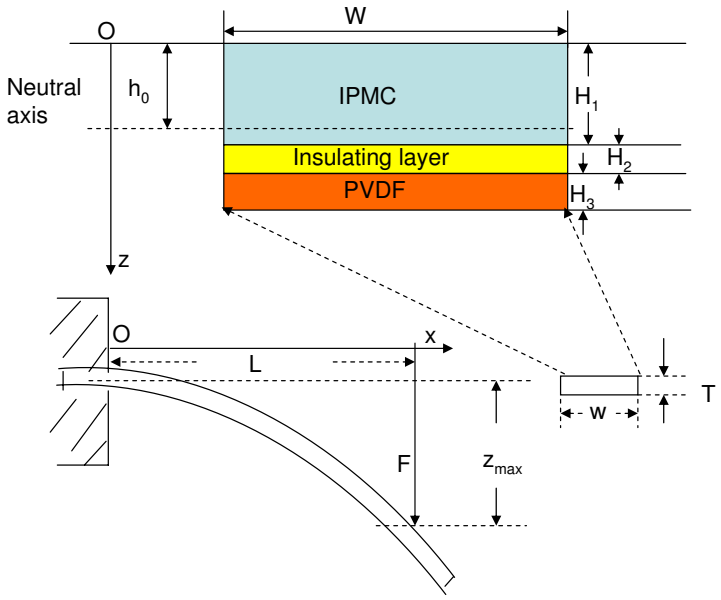

Figure 4. Bending of IPMC/PVDF composite beam.

Mitutoyo) is used to monitor the experiments. Fig. 5(a) illustrates the diagram of the experimental setup, while Fig. 5(b) shows the actual picture. Measurements are conducted for an IPMC beam and two IPMC/PVDF beams which have insulating layers in different thickness (IPMC/PVDF1 and IPMC/PVDF2). Detailed beam dimensions can be found in Table 1. Fig. 6 shows the measured displacement versus force data and the linear approximations, from which the spring constants can be calculated. From the experimental data, the Young's moduli of individual layers can be identified using (11): $E_1 = 0.571$ GPa, $E_2 = 0.73$ GPa, $E_3 = 1.96$ GPa. These values are within the ranges reported in the literature [21, 22].

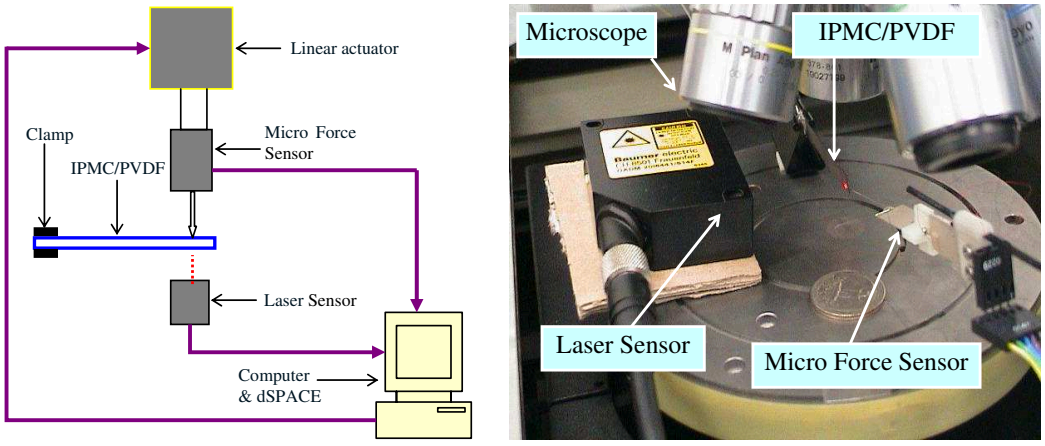

(a) (b)

Figure 5. (a): Experimental setup for spring constant measurement; (b): Picture of the experimental setup.

Table 1. Dimension and spring constant of different beams.

Beams	IPMC	IPMC/PVDF1	IPMC/PVDF2
W (mm)	7.3	8.2	7.6
L (mm)	37.2	36.0	33.0
H_1 (μm)	355	340	350.0
H_2 (μm)		30.0	100.0
H_3 (μm)		30.0	30.0
K_{mea} (N/m)	0.906	2.283	4.676
K_{FEA} (N/m)	0.908	2.286	4.647

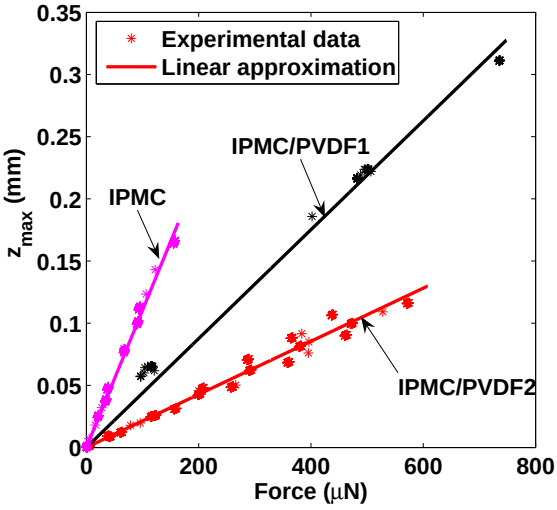

Figure 6. Spring constant of IPMC/PVDF beams.

To validate the linear analysis above, more accurate finite-element computation is conducted using CoventorWare, where the identified parameters are used together with the given geometric dimensions. The spring constants are calculated based on the free-end deflection of beams when they are subjected to an external force $F = 20$ μN at the tip. Table 1 lists the spring constants obtained through experimental measurement (K_{mea}) and finite element analysis (K_{FEA}), for the different beams. The close agreement between K_{mea} and K_{FEA} validates the model and analysis.

As shown in Table 1, the thicker the insulator, the stiffer the IPMC/PVDF structure. In order to optimize the bending performance of the IPMC/PVDF structure, one should select the elastic insulating layer as soft and thin as possible. However, thinner insulating layer may result in stronger electrical feedthrough coupling. In our design, the thickness of the insulating layer is chosen to be 30 μm to achieve tradeoff between the two considerations.

4. Electrical feedthrough coupling and model-based real-time compensation

4.1. The feedthrough coupling effect

Since the PVDF film is closely bonded to the IPMC with a very thin insulating PVC film, the coupling capacitance between the IPMC and the PVDF results in the electical feedthrough effect during simultaneous actuation and sensing. When the actuation signal is applied to the IPMC, the actuation voltage generates coupling current going through the insulating layer and then induces coupling charge on the PVDF. As a result, the charge amplifier gathers both the sensing and coupling charges from the PVDF. The presence of feedthrough coupling is illustrated by applying a 0.4 Hz square-wave actuation input (peak-to-peak 1.4 V). In the experiment, the humidity is 34% and the temperature is 23^{o}C. Fig. 7(a) shows the bending displacement detected by the laser sensor, while Fig. 7(b) shows the output from the charge amplifier. The spikes in the PVDF sensor output arise from the capacitive coupling between the IPMC and PVDF layers when the actuation voltage jumps.

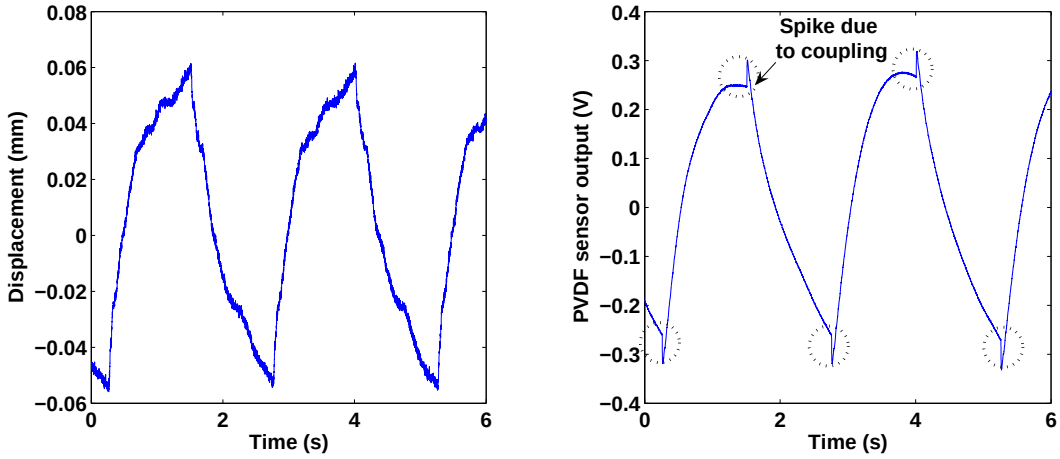

(a) (b)

Figure 7. (a): Bending displacement detected by the laser sensor; (b): Sensing output from the PVDF, showing the spikes from electrical feedthrough.

4.2. Modeling of the coupling effect

A complete circuit model of the IPMC/PVDF structure is developed to understand and capture the feedthrough coupling dynamics. As shown in Fig. 8, the model includes the equivalent circuits for individual layers and their natural couplings. Due to the non-negligible resistances resulted from the porous surface electrodes of the IPMC, the voltage potential is not uniform along the IPMC length. A distributed transmission-line type model is thus proposed. The overall circuit model is broken into discrete elements along its length for parameter identification and simulation purposes. In this paper,

the circuit model is chosen to have four sections of identical elements. The surface resistance of IPMC is represented by R_{s1}, while other key electrodynamic processes (e.g., ionic transport, polymer polarization, and internal resistances) are reflected in the shunt element consisting of resistor R_{c1} and capacitor C_{p1}. The polymer resistance is described by R_{p1}. In the circuit model of the insulating layer, R_{p2}, C_{p2}, R_{c2} are resistances and capacitances between the IPMC and PVDF. In the circuit model of the the PVDF, R_{s3} is the surface resistance of PVDF and R_{p3}, C_{p3} represent the resistance and capacitance between the electrodes of the PVDF.

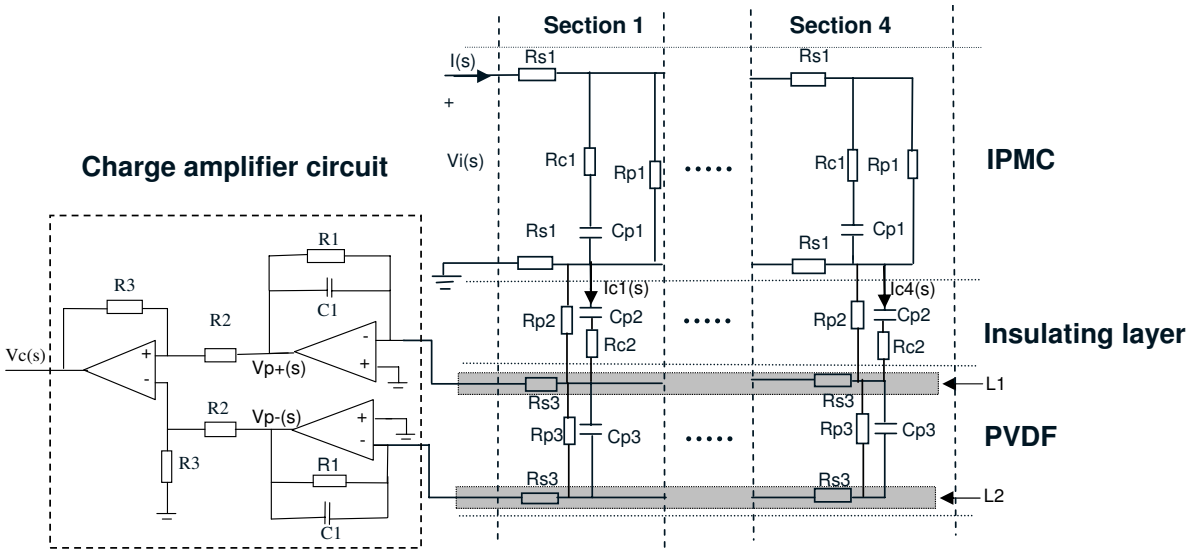

Figure 8. Circuit model of the IPMC/PVDF structure.

In order to identify the circuit parameters, the impedances are measured at multiple frequencies. The impedances of each layer are nonlinear functions of the resistances and capacitances involved. The parameters are identified using the Matlab command $nlinfit$, which estimates the coefficients of a nonlinear function using least squares. Table 2 lists the identified parameters.

Table 2. Identified parameters in the circuit model.

IPMC layer		Insulating Layer		PVDF layer	
R_{s1}	17 Ω	R_{p2}	500 MΩ	R_{s3}	0.1 Ω
R_{c1}	30 Ω	C_{p2}	42 pF	R_{p3}	600 MΩ
C_{p1}	3 mF	R_{c2}	4.5 MΩ	C_{p3}	290 pF
R_{p1}	25 KΩ				

The proposed circuit model will be validated by comparing its prediction of the feedthrough coupling signal with experimental measurement. We first explain a simple method for measuring the coupling signal. We observe that, due to the low surface resistance of PVDF (see Table 2), the electrode layer L_1 in Fig. 8 shields the coupling

current from reaching the electrode layer L_2. This means that the feedthrough coupling signal does not exist in V_{p-}, which is related to the charge from the layer L_2. This statement is supported by the measurement, shown in Fig. 9(a), where spikes only appear in V_{p+}. Since only V_{p+} has the coupling component while the sensing components in V_{p-} and V_{p+} have a phase shift of 180°, the coupling signal is obtained as:

$$V_c = V_{p+} + V_{p-}. \tag{12}$$

Fig. 9(b) shows the extracted coupling signal.

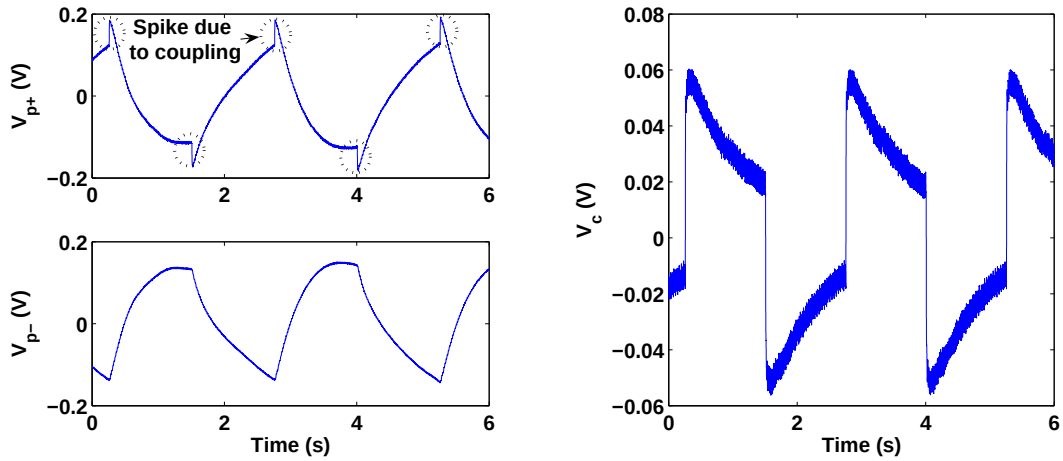

(a) (b)

Figure 9. (a) V_{p+}, V_{p-} sensing signals; (b) Extracted coupling signal V_c.

Fig. 10 compares the Pspice simulation results based on the circuit model with experimental results when a 1 Hz square-wave actuation voltage is applied. Good agreement is achieved for both the actuation current in IPMC (Fig. 10(a)) and the coupling voltage V_c (Fig. 10(b)).

The transfer function from the actuation voltage to the coupling voltage can be derived from the circuit model. Since there are 14 capacitors in the circuit model, the transfer function will be $14th$-order, which is not easy to implement in real time. After an order-reduction process, the transfer function of the coupling dynamics can be approximated by a 5th-order system:

$$T_c = \frac{-(509s^4 + 72s^3 + 1.5 \times 10^4 s^2 + 2203s)}{s^5 + 9525s^4 + 1.5 \times 10^4 s^3 + 2.9 \times 10^5 s^2 + 4.5 \times 10^5 s + 6 \times 10^4}. \tag{13}$$

To further verify the coupling model, a sequence of sinusoidal voltage signals with frequency ranging from 0.01 Hz to 20 Hz are applied to the IPMC. Actuation voltages are measured and coupling signals are effectively extracted from V_{p+} and V_{p-} for the purpose of obtaining the empirical Bode plots of coupling dynamics. Fig. 11 shows that the Bode plots of the derived transfer function (13) match up well with the measured Bode plots.

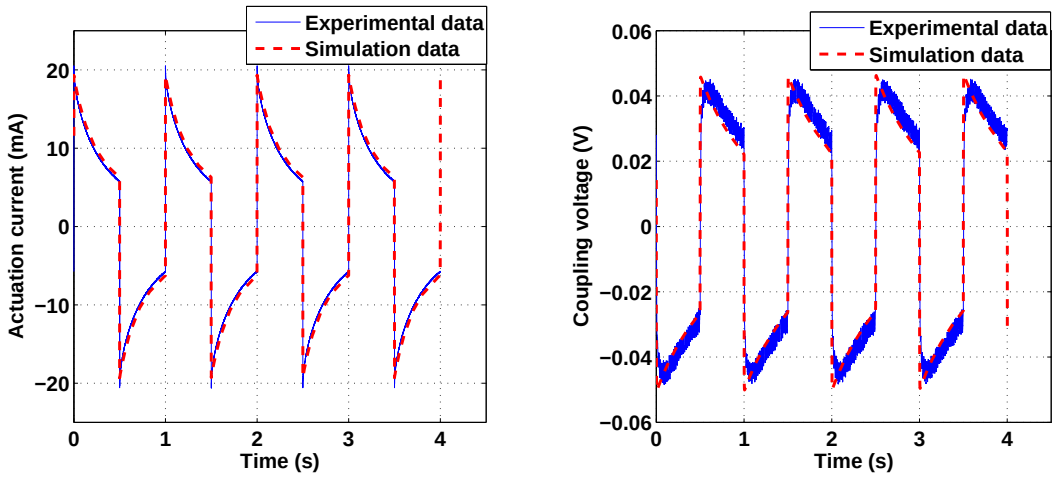

(a) (b)

Figure 10. Comparison of model prediction and experimental measurement. (a): Actuation current; (b): Coupling signal.

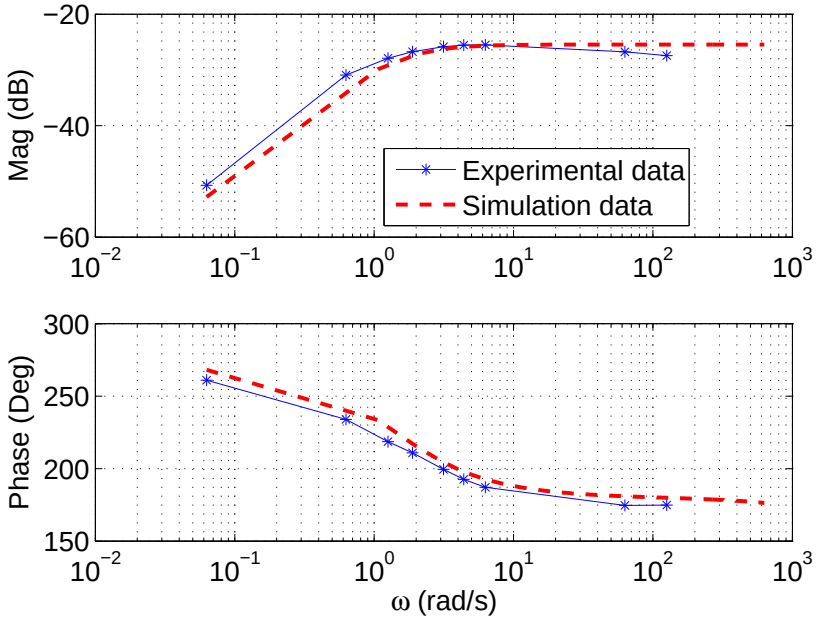

Figure 11. Verification of the coupling dynamics.

4.3. Real-time compensation in simultaneous actuation and sensing

There are several possible schemes to get rid of the coupling signal. Inserting another conductive layer between the IPMC and PVDF to shield the feedthrough coupling is one potential solution, but at the cost of increased stiffness and fabrication complexity. Another solution is to just use V_{p-} as the sensing signal, but this single-mode sensing scheme is sensitive to the common-mode noise in practice. Since the coupling dynamics has high-pass characteristics, one might also try to eliminate the coupling component

with low-pass filtering. However, the relatively low cut-off frequency of the coupling dynamics, comparing to the actuation bandwidth (See Fig. 12), makes this approach infeasible.

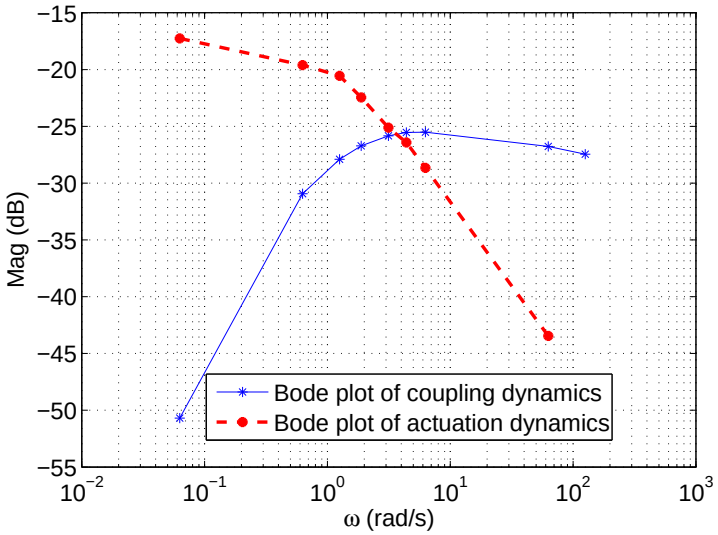

Figure 12. Bode plots of coupling dynamics and actuation dynamics.

In this paper, a model-based real-time compensation scheme is proposed to remove the feedthrough coupling component. The coupling charge is calculated from the coupling circuit model (13). By subtracting it from the measured charge of the PVDF, the sensing charge can be extracted. Fig. 13 illustrates the compensation scheme. Fig. 14 compares the displacement measurement obtained from the PVDF sensor with that from the laser sensor when a 0.4 Hz square-wave actuation input is applied. It is seen that the spike related to the electrical coupling is removed by the compensation scheme. Although there is about 12% error shown in Fig. 14, the amplitudes and the phases agree well. Investigation is under way to further improve the measurement accuracy of the PVDF sensor.

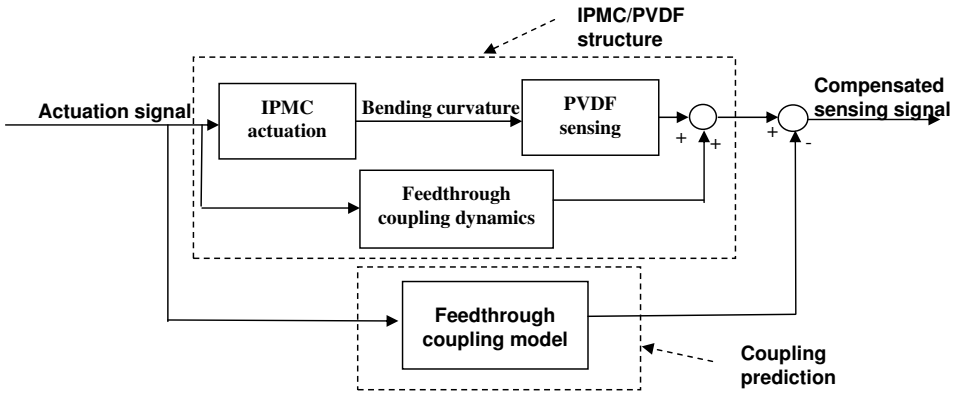

Figure 13. Diagram of the real-time compensation.

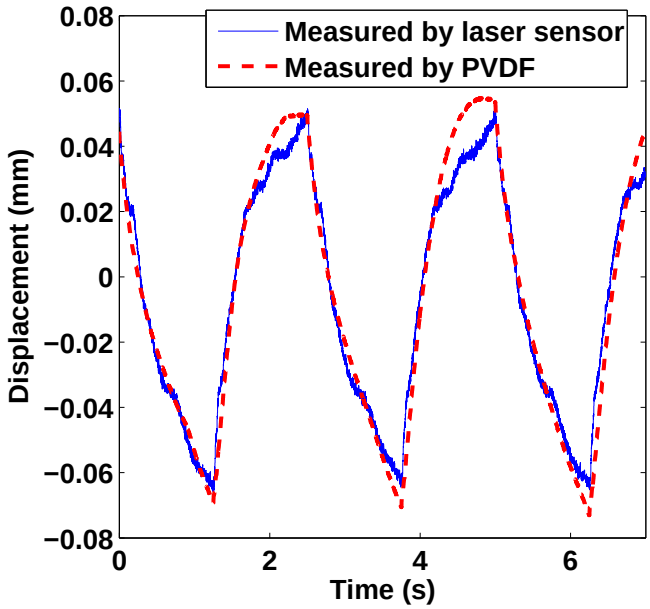

Figure 14. Comparison of displacement measurements by laser sensor and PVDF sensor.

5. Application to micro-injection of living Drosophila embryos

The developed IPMC/PVDF sensori-actuator is applied to the micro-injection of living Drosophila embryos. Such operations are important in embryonic research for genetic modification. Currently this process is implemented manually, which is time-consuming and has low success rate due to the lack of accurate control on the injection force, the position, and the trajectory. The IPMC/PVDF structure is envisioned to provide accurate force and position control in the micro-injection of living embryos, and thus to automate this process with a high yield rate. In this paper, an open-loop injection experiment with the IPMC/PVDF sensori-actuator is conducted, and the process of the injection behavior is captured by the PVDF sensor.

The developed IPMC/PVDF micro-force injector is illustrated in Fig. 15. A micro pipette with an ultra-sharp tip (1.685 μm in diameter and 2.65^{o} in angle), is mounted at the end point of a rigid tip attached to the IPMC/PVDF structure.

The Drosophila embryos are prepared as described in [23]. The dimensions of the embryos are variable with an average length of 500 μm and a diameter of about 180 μm. Fig. 16(a) shows the diagram of the experimental setup for embryo injection, while Fig. 16(b) shows the photo. A 3-D precision probe station (CAP-945, Signatone), which is controlled by a 3-D joystick, moves the needle close to an embryo and then a ramp voltage, which starts from 0 V and saturates at 2 V, is applied to the IPMC. The IPMC drives the beam with the needle to approach the embryo. After the needle gets in contact with the membrane of the embryo, the latter will be deformed but not penetrated due to its elasticity. At this stage, the needle is still moving until the reaction

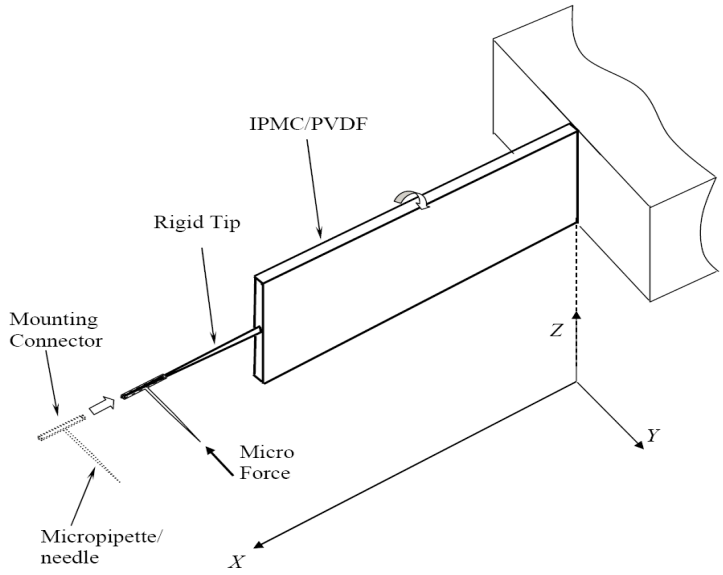

Figure 15. Illustration of the IPMC/PVDF micro-force injector.

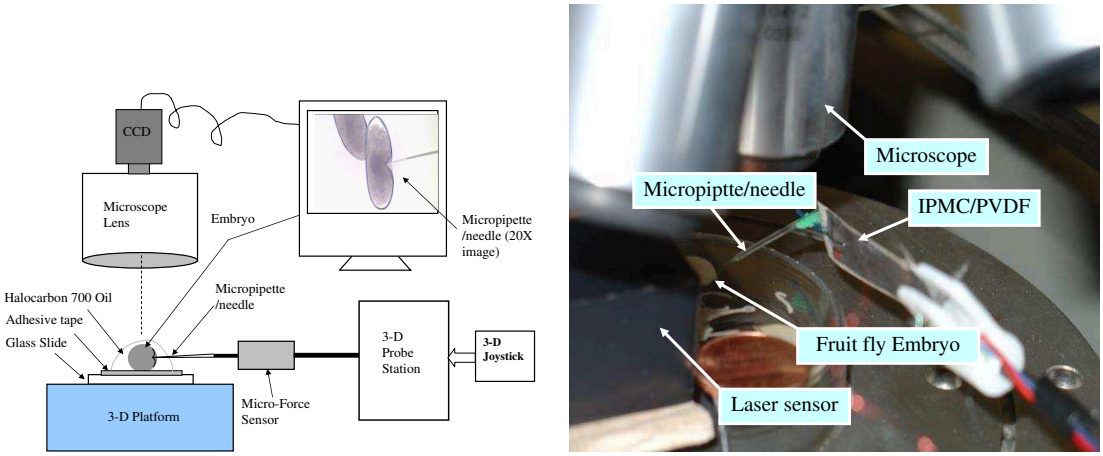

(a) (b)

Figure 16. (a): Diagram of experimental setup for embryo injection; (b): Picture of experimental setup.

force between the needle and embryo reaches the penetration force. The needle stops at the penetration moment for a while (about 0.2 ms) due to temporary force balance. After that, the embryo membrane is penetrated and the needle moves freely into the embryo.

Fig. 17(a) shows the snapshots of the successful injection progress. Fig. 17(b) shows both the displacement of the needle detected by the laser sensor and by the compensated PVDF sensing signal. It is concluded that the predicted displacement reflects the movement of the needle, and the process of injection can be monitored by the PVDF.

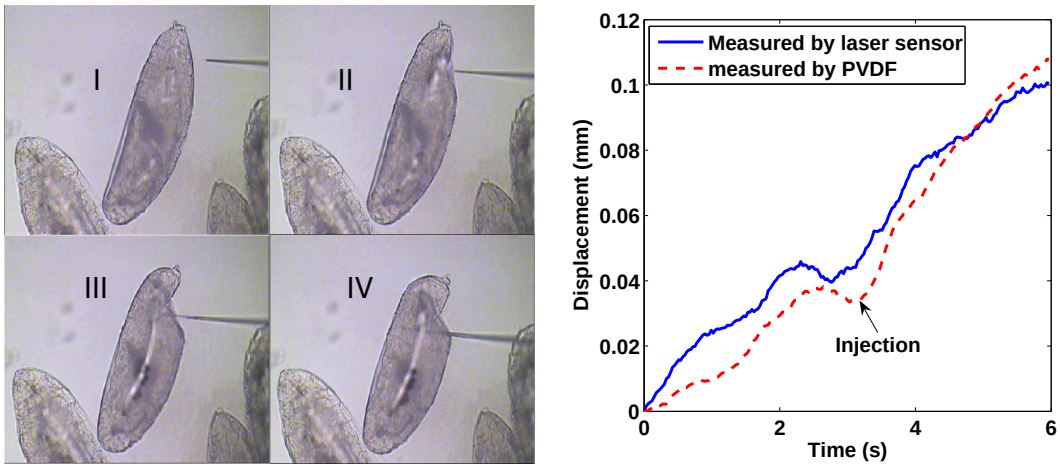

(a) (b)

Figure 17. (a): Snap shots captured during the embryo injection; (b): Bending displacement during the injection measured by both the laser sensor and the integrated PVDF sensor.

6. Conclusions and future work

In this paper, a novel hybrid IPMC/PVDF structure is developed for both micro sensing and actuation. The feedthrough coupling effect from actuation signal to sensing signal is addressed through optimization of the insulating layer thickness and model-based compensation. Experimental results demonstrate that the developed IPMC/PVDF sensori-actuator, together with the model-based compensation algorithm, can perform effective, simultaneous actuation and sensing. As the first application, the sensori-actuator has been successfully used for open-loop micro injection of Drosophila embryos. The penetration process is captured well by the compensated PVDF sensing signal.

The model-based compensation algorithm assumes a fixed model for feedthrough dynamics. For an IPMC based on water solvent, the feedthrough dynamics is expected to change with the hydration level of IPMC. In other words, the coefficients in the model (13) will be time-varying. In this case recursive estimation methods [24] can be used to update the model online based electrical measurement. On the other hand, if one uses an IPMC that has stable performance in air (based on different solvent than water), compensation using a fixed model will suffice.

Ongoing research is focused on investigation of nonlinear, dynamic behavior of PVDF as well as the thermal drift associated with the pyroelectric effect of PVDF, with a goal of improving the measurement accuracy of the PVDF sensor. The IPMC/PVDF configuration in this paper allows only the sensing of the bending displacement (or curvature). This will be extended to integrated sensing of both displacement and force output, which is of importance in numerous biological micromanipulation applications. Finally, feedback of the control of embryo injection will be studied to fully automate

the process.

Acknowledgments

This research was supported in part by an NSF SGER grant (CMS 0550651), an NSF CAREER grant (ECS 0547131), MSU IRGP (05-IRGP-418), and a Summer Dissertation Fellowship awarded to Z. Chen by the MSU Graduate School and by Microsoft Inc. The contribution of Jason Malinak to the early-stage development of the IPMC/PVDF structure is also acknowledged. The authors would like to thank Mr. Martin S. Buckley and Miss Li Li at the Arnosit's Lab of Department of Biochemistry & Molecular Biology, MSU for their great effort on the preparation of fresh Drosophila embryos.

References

[1] Y. Bar-Cohen, "Electric flex," *IEEE Spectrum*, vol. 41, no. 6, pp. 29–33, 2004.

[2] M. Shahinpoor and K. J. Kim, "Ionic polymer-metal composites: I. fundamentals," *Smart Materials and Structures*, vol. 10, pp. 819–833, 2001.

[3] S. Guo, T. Fukuda, and K. Asaka, "A new type of fish-like underwater microrobot," *IEEE/ASME Transactions on Mechatronics*, vol. 8, no. 1, pp. 136–141, 2003.

[4] B. Kim, J. Ryu, Y. Jeong, Y. Tak, B. Kim, and J.-O. Park, "A ciliary based 8-legged walking micro robot using cast IPMC actuators," in *Proceedings of IEEE International Conference on Robots and Automation*, 2003, pp. 2940–2945.

[5] S. Guo, T. Fukuda, K. Kosuge, F. Arai, and M. Negoro, "Micro catheter system with active guide wire," in *Proceedings of IEEE International Conference on Robotics and Automation*, 1995, pp. 79–84.

[6] Y. Bar-Cohen, S. Leary, M. Shahinpoor, J. O. Harrison, and J. Smith, "Flexible low-mass devices and mechanisms actuated by electroactive polymers," in *Smart Structures and Materials 1999: Electroactive Polymer Actuators and Devices*, ser. Proceedings of SPIE, Y. Bar-Cohen, Ed., vol. 3669. Bellingham, WA: SPIE, 1999, pp. 51–56.

[7] S. Tadokoro, S. Yamagami, and M. Ozawa, "Soft micromanipulation device with multiple degrees of freedom consisting of high polymer gel actuators," in *Proceedings of IEEE International Conference on Micro Electro Mechanical Systems*, 1999, pp. 37–42.

[8] R. Lumia and M. Shahinpoor, "Microgripper design using electroactive polymers," *Smart Structures and Materials 1999: Electroactive Polymer Actuators and Devices*, pp. 322–329, 1999.

[9] J. Dosch, D. Inman, and E. Garcia, "A self-sensing piezoelectric actuator for collocated control," *Journal of Intelligent Material Systems and Structures*, vol. 3, pp. 166–185, 1992.

[10] C. Bonomo, C. D. Negro, L. Fortuna, S. Graziani, and D. Mazza, "Characterization of IPMC strip sensorial properties: Preliminary results," in *Proceedings of International Symposium on Circuits and Systems*, 2003, pp. IV–816–IV–819.

[11] K. Farinholt and D. Leo, "Modeling of electromechanical charge sensing in ionic polymer transducers," *Mechanics of Materials*, vol. 36, pp. 421–433, 2004.

[12] K. M. Newbury, "Characterization, modeling, and control of ionic polymer transducers," Ph.D. dissertation, Virginia Polytechnic Institute and State University, 2002.

[13] Measurement Specialties, *Piezo Film Sensors Technical Manual*, Hampton, VA, 1998.

[14] K. Y. Lam and T. Ng, "Active control of composite plates with integrated piezoelectric sensors and actuators under various dynamic loading conditions," *Smart Materials and Structures*, vol. 8, pp. 223–237, 1999.

[15] Y.-S. Lee, S. J. Elliot, and P. Gardonio, "Matched piezoelectric double sensor/actuator pairs for beam motion control," *Smart Materials and Structures*, vol. 12, pp. 541–548, 2003.

[16] E. Wieschaus, "From molecular patterns to morphogenesis: The lessons from Drosophila," in *Nobel Lectures, Physiology or Medicine 1991-1995*, N. Ringertz, Ed. World Scientific Publishing Co., 1997.

[17] Measurement Specialties, *Piezo Film Sensors Technical Manual*, Hampton, VA, 1999.

[18] M. D. Bennett and D. Leo, "Ionic liquids as stable solvents for ionic polymer transducers," *Sensors and Actuators A: Physical*, vol. 115, pp. 79–90, 2004.

[19] Y. Shen, N. Xi, U. Wejinya, and W. Li, "High sensitivity 2-D force sensor for assembly of surface MEMS devices," in *Proceedings of IEEE/RSJ International Conference on Intelligent Robots and Systems*, Sendai, Japan, 2004, pp. 3363–3368.

[20] J. M. Gere and S. Timoshenko, *Mechanics of Materials*, 4th ed. Boston, MA: PWS Publishing Company, 1997.

[21] M. Siripong, S. Fredholm, Q. Nguyen, B. Shih, J. Itescu, and J. Stolk, "A cost-effective fabrication method for ionic polymer-metal composites," in *Electroresponsive Polymers and Their Applications*, ser. MRS Symposium Proceedings, V. Bharti, Y. Bar-Cohen, Z. Cheng, Q. Zhang, and J. Madden, Eds., vol. 889, Warrendale, PA, 2006, pp. 0889–W04–03.

[22] T. Sakakibara, H. Izu, T. Kura, W. Shinohara, H. Iwata, S. Kiyama, and S. Tsuda, "Development of high-voltage photovoltaic micro-devices for an energy supply to micromachines," in *Proceedings of IEEE 5th International Symposium on Micro Machine and Human Science*, Nagoya, Japan, 1994, pp. 71–76.

[23] Y. Shen, U. C. Wejinya, N. Xi, M. S. Buckley, C. A. Pomeroy, and D. N. Arhosti, "Force measurement and mechanical characterization of living Drosophila embryos for human medecal study," *Journal of Engineering in Medicine*, 2006, sumitted.

[24] K. J. Astrom and B. Wittenmark, *Adaptive Control*, 2nd ed. Addison-Wesley, 1995.